



Contents lists available at ScienceDirect



Catalysis Today

journal homepage: www.elsevier.com/locate/cattod

Characterization and catalytic performance of Co-Mo-W sulfide catalysts supported on SBA-15 and SBA-16 mechanically mixed

M.A. López-Mendoza^a, R. Nava^b, C. Peza-Ledesma^a, B. Millán-Malo^a, R. Huirache-Acuña^c, P. Skewes^a, E.M. Rivera-Muñoz^{a,*}

^a Centro de Física Aplicada y Tecnología Avanzada, Universidad Nacional Autónoma de México, Departamento de Nanotecnología, A.P. 1-1010 Querétaro, Qro. C.P. 76000, Mexico

^b Facultad de Ingeniería, Universidad Autónoma de Querétaro, Centro Universitario, Cerro de las Campanas, 76010, Querétaro, Mexico

^c Facultad de Ingeniería Química, Universidad Michoacana de San Nicolás de Hidalgo, Ciudad Universitaria, 58060, Morelia, Michoacán, Mexico

ARTICLE INFO

Article history:

Received 26 March 2015

Received in revised form 23 July 2015

Accepted 28 July 2015

Available online xxx

Keywords:

HDS catalysts

Mesoporous silicas

SBA-15

SBA-16

ABSTRACT

A group of hydrodesulfurization (HDS) catalysts, based on transition metal sulfides (Co-Mo-W) and supported on mechanically-mixed mesoporous silicas (SBA-15 and SBA-16), have been synthesized and characterized by physicochemical methods (DRS-UV-vis, Micro Raman spectroscopy, XRD, SEM, HRTEM, EDS and catalytic activity). It has been demonstrated that the use of a mixture of silicas with two different porous structures has an advantage with respect to the use of the SBA-15 and SBA-16 separately for the preparation of supported catalysts for hydrodesulfurization reactions of refractory sulfur compounds, such as dibenzothiophene. This is because the presence of different porous structures has a positive effect over the diffusion processes of the precursors of the active phases on the support, and the whole result is a higher catalytic activity for the HDS reactions of dibenzothiophene, even more than that of the commercial catalyst used as a comparative model; this activity is also related with the stage of the synthesis process in which the mixture is done.

© 2015 Elsevier B.V. All rights reserved.

1. Introduction

Currently, oil and its derivatives, natural gas and coal are the main sources of primary energy worldwide and this tendency will not change in the next two decades according to recent studies in energy topics.

Currently, oil and its derivatives are, along with natural gas and coal, the main sources of primary energy worldwide and, according to recent studies, this tendency will continue for the next two decades [1]. It involves a great quantity of challenges related to the separation of the fractions in the oil, specifically those associated with the removal of undesired elements such as nitrogen, oxygen, sulfur and metals, because of the environmental effects of those compounds. Hydrodesulfurization (HDS) focuses in the removal of sulfur-containing molecules in oil, typically by the use of catalytic materials. In the recent years, the research in this topic has focused its efforts in the development of new catalysts, which has to be effective in the removal of molecules of complex compounds of

sulfur such as thiophenes and benzothiophenes which are difficult to remove with conventional commercial catalysts.

The most of the catalytic materials used in hydrotreatment processes are based on transition metal sulfides, typically those of molybdenum and tungsten, promoted by cobalt or nickel and supported in inert materials. Alumina is the most common support material for HDS reactions for their mechanical properties, low cost and easy regeneration; however, this material has several disadvantages, mainly related to the presence of undesired interactions between transition metal and support which has promoted the research of alternative materials such as titania and silica, which latter have demonstrated alumina equally advantageous properties in terms of physical and chemical properties. Numerous previous studies have reported the convenience of using mesoporous silicas with cubic (SBA-16) or hexagonal (SBA-15) mesostructure as a support material for active species to be used in the hydrodesulfurization reactions since they have shown outstanding performance for the removal of sulfur atoms within the molecular structure of thiophenes and benzothiophenes.

Different mesoporous silica materials have been studied as supports for hydrodesulfurization catalysts, such as MCM, HMS and SBA materials, because of their ordered porous structure and high surface area. Particularly, many studies have been published

* Corresponding author. Tel.: +52 4422381158; fax: +52 4422381165.

E-mail addresses: erivera@unam.mx, emrivera@fata.unam.mx

(E.M. Rivera-Muñoz).

regarding the use of SBA type materials as catalyst supports for the HDS reactions. According to the studies by Nava and co-workers [2–6], the SBA-15 and SBA-16 materials are suitable supports for depositing transition metal sulfides enabling the synthesis of bimetallic and trimetallic catalysts, which have demonstrated greater activity than commercial catalysts supported on alumina. Similar results have been reported by Soni and co-workers who have synthesized NiMo catalyst supported on SBA-15 and SBA-16 which have been tested in different hydrotreatment reactions showing a good activity and obtaining a better performance for those supported on SBA-16 [7,8]. Meanwhile, Klimova and co-workers have used SBA-15 and SBA-16 silicas as catalytic support for the system Ni-Mo-W under different conditions obtaining improvement in catalytic activity for hydrodesulfurization of dibenzotriophene-like molecules [9–11]. Adjaye and co-workers have proven the effectiveness of SBA-15 as support for HDS catalysts using system Ni-Mo and Fe-W obtaining catalytic activities comparable to those of commercial NiMo-alumina catalysts [12,13]. Rayo and co-workers have studied the effect of the acid-base conditions of the impregnation media and the presence of dopant heteroatoms such as Al, Ti and Zr over Ni-Mo sulfided catalysts supported in SBA-15 used in the HDS reaction of thiophene, obtaining good catalytic performance, improved by the presence of conditions or heteroatoms capable to promote an increase the Brønsted acidity in the catalyst surface and avoid the NiMoO₄ formation, additionally they have reported that the synthesis of transition metal sulfide precursors under acid conditions favors the preservation of the porous structure of the SBA-15 [14,15].

Additional studies have focused on the surface modification/functionalization of the SBA materials by incorporation of other transition metals such as titania, zirconia or alumina, observing an improvement in the dispersion and reducibility of the active species, which results in a better catalytic performance [2,5,16–18]. Wang and co-workers have demonstrated the importance of porous morphology in catalysts supported in mesoporous silica SBA-15 by the synthesis of materials with different structure showing different catalytic performance as consequence of differences in the diffusion processes in the porous structure [19].

Despite all these studies, to date there have been no reported research on the combination of supports, with different porosities, for transition metal sulfides, HDS catalysts.

In this work, a group of HDS catalysts, based on transition metal sulfides (Co-Mo-W), supported in mixtures of mesoporous silicas (SBA-15 and SBA-16) have been synthesized and characterized by different physicochemical techniques in order to determine their catalytic properties and performance.

2. Materials and methods

2.1. Support preparation

The siliceous SBA-15 and SBA-16 mesoporous materials were synthesized according to the procedure described previously by Zhao et al. [20] and Flodström and Alfredsson [21]. For the synthesis of SBA-15 material, Pluronic® P-123 (EO₂₀PO₇₀EO₂₀, Sigma-Aldrich) triblock copolymer was used as the structure-directing agent. In a typical synthesis, the Pluronic® P-123 was completely dissolved in a solution of water and HCl 4 M under stirring. After that, the required amount of tetraethyl orthosilicate (TEOS, 98%, Sigma-Aldrich) was added to the solution, the sol-gel reaction was carried out with stirring at 35 °C for 24 h. The reaction mixture was subsequently transferred into polypropylene bottles and heated at 80 °C for 24 h in a controlled-temperature

oven. Afterward, the obtained solid was vacuum filtered, washed thoroughly with deionized water and dried first in air at room temperature and then at 110 °C for 18 h and finally calcined at 500 °C for 6 h in a static air muffle with a 2 °C per minute temperature ramp, in order to remove the organic template.

A very similar procedure was used to synthesize the SBA-16 support where Pluronic® F-127 (EO₁₀₆PO₇₀EO₁₀₆, Sigma-Aldrich) triblock copolymer was used as the structure directing and completely dissolved in the corresponding amount of HCl 2 M under stirring. After total dissolution, TEOS was added and allowed to react at 28 °C for 20 h. Then, the reaction mixture was transferred into polypropylene bottles and heated at 80 °C for 48 h in oven. The solid residue was vacuum filtered, washed thoroughly with deionized water and dried at room temperature and then at 110 °C for 18 h. Finally, the sample was calcined at 500 °C in a static air muffle with a 2 °C per minute temperature ramp, for 6 h for the removal of the copolymer.

The catalytic supports based on mesoporous silicas were obtained by the mechanical mixing of equal molar quantities of SBA-15 and SBA-16 materials. For the preparation of the mixtures pure silicas were meshed in Tyler Standard Meshes No. 120 and 150 in order to obtain product with particle sizes between 106 and 125 µm; meshed silicas were blended by hand during 15 min in order to achieve a complete incorporation of the two silicas. Supports were mixed in three different ways: a blend was made prior to the impregnation of the active phase precursors (MMIC – Mechanical Mixture + Impregnation + Calcination), another one after the impregnation of SBA-15 and SBA-16 separately but before calcination (IMMC – Impregnation + Mechanical Mixture + Calcination) and finally, after separate impregnation and calcination of SBA-15 and SBA-16 supports (ICMM – Impregnation + Calcination + Mechanical Mixture).

2.2. Catalysts preparation

Oxide-state catalysts were prepared by the simultaneous impregnation via incipient wetness method. Each support was loaded with fixed equal amounts of molybdenum (5.75 wt% as MoO₃), tungsten (10.92 wt% as WO₃) and cobalt (3.05 wt% as CoO). In a typical synthesis, 1 g of support was impregnated with 1 mL of impregnation aqueous solution containing ammonium heptamolybdate tetrahydrate ((NH₄)₆Mo₇O₂₄·4H₂O, assay: 81–83%, Sigma-Aldrich), ammonium metatungstate hydrate ((NH₄)₆H₂W₁₂O₄₀·xH₂O, assay: 99%, Sigma-Aldrich) and cobalt nitrate hexahydrate (Co(NO₃)₂·6H₂O, assay: 98%, Sigma-Aldrich). The concentrations of each transition-metal precursor were calculated to achieve a Mo(W)/(Mo + W) atomic ratio of 0.5 and a Co/(Mo + W) atomic ratio of 0.43. The impregnated supports were dried first at room temperature for 5 h and then at 85 °C for 16 h. Finally, they were calcined at 500 °C for 4 h in a static air muffle with a 2 °C per minute temperature ramp. It is important to mention that the aqueous solution containing the precursors of the three metals is stable during preparation of the catalysts.

Fresh sulfided catalysts were prepared by sulfidation of the oxide-state catalysts. The sulfidation reaction was carried out in a U-shaped glass tubular reactor; oxide-state catalysts were charged in the reactor and heated until 400 °C in N₂ at 2 °C per minute; when reaction temperature was raised, sulfidation was carried out using a stream of 15 (v/v)% of H₂S in H₂ with a flux of 0.71 m³ per minute per catalyst gram, at controlled constant temperature (400 °C) for 4 h. Once the sulfidation reaction was carried out, sulfided catalysts were cooled to room temperature in a nitrogen stream and charged directly to the HDS reactor in inert atmosphere in order to avoid oxidation of the transition metal sulfides.

2.3. Characterization techniques

2.3.1. Scanning electron microscopy

Morphological properties of supports and catalysts were studied by scanning electron microscopy. Images for supports and oxide-state catalysts were obtained using secondary electrons in a JEOL JSM-6060 LV microscope operated at 20 kV under high vacuum conditions. Samples were ground into a fine powder and deposited over copper stubs and covered with a thin gold film with the aid of a metal evaporator EMS 550 Sputter Coater. Sulfided catalysts were characterized with a JEOL JSM-7600F microscope operated at 1 kV and under high vacuum and by the use of secondary electrons for the collection of images; powdered samples were treated in an inert atmosphere and deposited on copper stubs and analyzed in an uncoated way.

2.4. Chemical analysis

The chemical analysis of the oxide-state and fresh sulfided catalysts (wt%) was determined by energy-dispersive X-ray spectroscopy (EDS); oxide-state catalysts were analyzed with a Oxford Inca X-Sight system taking into account the average of five measurements in different points of the samples. Elemental distribution maps and composition of fresh sulfided catalysts were recorded in a similar system making a complete scanning of the samples.

2.5. Nitrogen adsorption-desorption studies

The textural properties of the catalysts and supports were determined from the adsorption-desorption isotherms of nitrogen at 77 K, recorded with a Quantachrome Autosorb iQ2 instrument. Prior to the analysis, the samples were degassed at 200 °C in vacuum (0.2 atm) for 12 h. The volume of the adsorbed N₂ was normalized to the standard temperature and pressure. The specific surface area of the samples was calculated by applying the BET method taking into account the nitrogen adsorption data within the 0.05–0.30 relative pressure range. The pore diameter distribution was calculated by the BJH method using the desorption branch of the isotherms. The accumulated pore volume was obtained from the adsorption-desorption isotherms for a relative pressure (P/P_0) of 0.99.

2.6. Small-angle X-ray diffraction

The ordered mesoporous structure of the supports was investigated by small-angle X-ray diffraction in the 0.5–5° range for 2θ . Samples were analyzed on a Rigaku Ultima IV diffractometer, using Ni-filtered Cu-K α radiation ($\lambda = 1.54 \text{ \AA}$), operated at 40 kV and 30 mA and with a step size of 5° per minute and scanning every 0.02 s, with rotation of the specimen at 30 revolutions per minute.

2.7. Wide-angle X-ray diffraction

The presence of crystalline phases of oxides and sulfides of transition metals in the catalysts was determined by X-ray diffraction in the 5–80° range for 2θ ; diffractograms for oxide-state catalysts were recorded in a Rigaku Miniflex diffractometer, using Ni-filtered Cu-K α radiation ($\lambda = 1.54 \text{ \AA}$), operated at 30 kV and 15 mA, with a step size of 2° per minute and sampling every 0.02 s.

Those for fresh sulfided catalysts were obtained in a Rigaku Ultima IV diffractometer, working with Co-filtered Cu-K α radiation ($\lambda = 1.54 \text{ \AA}$), with a step size of 5° per minute and sampling every 0.02 s and rotating the specimen at 30 revolutions per minute. The determination of the crystalline phases and indexing was done using the MDI -Jade® V 5.0.37 software.

2.8. DRS-UV-vis spectroscopy

Diffuse reflectance spectroscopy in the UV-visible range was aimed to determine the coordination environment of transition metals in oxide-state catalysts, spectra were recorded in the range of 200–800 nm at room temperature using a Varian Cary 5000 UV-vis spectrometer equipped with an integration sphere. Spectra were determined using an internal MgO reference material and using the SBA-15 as blank in order to avoid the appearance of the electronic transitions corresponding to the siliceous material. Before the analysis, samples were meshed in order to obtain particles with size in the range of the 100–125 μm .

2.9. Micro Raman spectroscopy

The characterization and aggregation of transition metal oxides in catalysts was studied by Micro-Raman spectroscopy, spectra were recorded at room temperature in a Dilor Labram II Micro-Raman system equipped with an Ar laser emitting at 488 nm and operated at 30 mW, with a resolution of $\pm 1 \text{ cm}^{-1}$, and a holographic notch filter from Kaiser Optical Systems, Inc. (model Super Notch-Plus).

2.10. Catalytic performance measurements

HDS reaction of DBT was carried out in a Parr model 4848 high pressure batch reactor. In order to minimize internal diffusion limitations, all catalysts were thoroughly ground in a mortar to a fine powder and meshed for use materials with particle size between 106 and 125 μm . For the experiment 0.5 g of sulfided catalyst were introduced into the batch reactor containing a solution of DBT in hexadecane with a concentration of 12 mmol/L at room temperature. The reactor was heated up to 320 °C in presence of inert atmosphere with N₂ (at an initial pressure of 200 psi). Once reaction temperature was raised, nitrogen was purged out and the reactor was pressurized with hydrogen to 800 psi, hydrodesulfurization reaction was carried out at constant temperature (320 °C) with intense stirring (700 rpm). These conditions allow to exclude external diffusion effects and minimize internal diffusion limitations [2,4,24–26]. The reaction time was averaged to 5 h from the incorporation of hydrogen to the reaction system. The residual reactants and resulting products concentrations were analyzed using gas chromatography by the use of an Agilent Technologies 7990A chromatograph provided with a 30-m packed column containing 3% OV-17 as separating phase.

Catalytic performance was measured taking into account two parameters: the apparent rate constant (related with the rate of reaction) and selectivity (related with the capability of the catalyst to promote the formation of desirable products). Apparent rate constant is a good approximation to the reaction rate in the sense that it involves the effect of the concentration of reactants and products, the effect of temperature and the negative effect of the presence of the H₂S in the batch reactor. Previous studies have shown that HDS reactions of simple sulfur compounds follows a pseudo-first order kinetics [19,22–26], so the apparent rate constants (k_{app}) were calculated by this model (Equation (01), where r_{HDS} is the reaction rate for the global HDS reaction, k_{app} is the apparent rate constant and [DBT] is the DBT concentration along the time) and assuming pseudo-zero order respect to hydrogen, under the consideration that an excess of hydrogen was employed, thus, its partial pressure could be considered as constant during the overall reaction time. Apparent reaction constants were calculated using an exponential fit of the DBT concentration data and a linearization of this fitting according to Equation (02), where [DBT]₀

represents the initial concentration of DBT and X_{DBT} is the DBT conversion at overall reaction time.

$$r_{HDS,app} = \frac{d[DBT]}{dt} = k_{app}[DBT] \quad (01)$$

$$[DBT]_0(1 - X_{DBT}) = k_{app}t \quad (02)$$

HDS of DBT can occur by two parallel pathways: direct desulfurization (DDS) and hydrogenation (HYD); the first leads to the formation of biphenyl (BP) via hydrolysis, this is, the sulfur atom is removed from the molecule by the breaking of the carbon–sulfur bonds, while the hydrogenation of one or two aromatic rings produces cyclohexylbenzene (CHB) and bicyclohexyl (BCH), respectively. The ability of the catalyst to promote preferably one of the two routes is known as selectivity and in this study was determined as the ratio between the generated quantities of hydrogenation products over those of direct desulfurization at conversion of 30% for dibenzothiophene according to the Equations (03)–(05), where the factors in brackets are the quantities of the HDS products.

$$DDS = \frac{[BP] \times 100}{[CHB] + [BCH] + [BP]} \quad (03)$$

$$HYD = \frac{[CHB] + [BCH]}{[CHB] + [BCH] + [BP]} \times 100 \quad (04)$$

$$\text{Selectivity} = \frac{HYD}{DDS} \quad (05)$$

For comparative purposes, in the reaction experiments were used equal catalyst mass, with similar particle size (100–125 μm) and with the same metal charge (added during catalysts synthesis); in addition, the HDS performance of a commercial CoMo/Al₂O₃ catalyst was measured as comparative model (Mo = 14.2%; Co = 3.8%; P = 0.83%; $S_{BET} = 223 \text{ m}^2/\text{g}$; average pore diameter = 6.6 nm).

3. Results and discussion

3.1. Nitrogen adsorption–desorption studies

Fig. 1 shows the obtained nitrogen adsorption–desorption isotherms at 77 K for the synthesized supports, it can be seen that all the supports show nitrogen adsorption–desorption Type-IV isotherms, according to the classification of the IUPAC [27–29], which are characteristic of mesoporous materials, with a hysteresis loop due to capillary condensation and evaporation within the mesopores. In the case of the SBA-15 material, it shows a type H1 hysteresis loop (according to IUPAC rules, [28,29]) in the range of

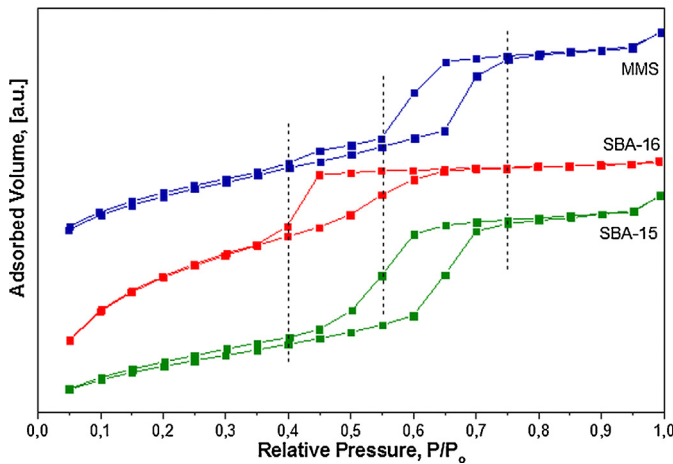


Fig. 1. Nitrogen adsorption–desorption isotherms for synthesized supports (MMS – mechanical mixture of mesoporous silicas).

relative pressures 0.40–0.75, in which the adsorption and desorption branches of the isotherm are substantially parallel, which is indicative of the presence of mesopores with regular shape, thus agreeing with the presence of cylindrical mesoporous channels in an hexagonal two-dimensional arrangement, typical of the SBA-15. This type of isotherm has been widely reported in previous studies of this material [4,20,21,30].

Meanwhile, the SBA-16 shows a H2 Type hysteresis loop in the range of relative pressures of 0.39–0.65 [28,29], in which the desorption branch is wider and vertical than that of adsorption, related with the presence of mesopores with non-uniform shape, which is consistent with the fact that this material is characterized by the presence of mesopores in the form of interconnected spheres, creating differences between the inlet and the pore diameters; this isotherm has also been widely documented in previous studies [4,20,21].

The mechanical mixture of mesoporous silicas (MMS) clearly shows two hysteresis loops, as expected considering that it consists of SBA-15 and SBA-16, the first one in the range of relative pressures of 0.40–0.55, which can be classified as H2 type according to the IUPAC rules [28,29], so that this first hysteresis loop is mainly related to the SBA-16 present in the mixture; the second hysteresis occurs in the range of relative pressures between 0.55 and 0.75, and clearly corresponds to an H1 type hysteresis loop [28,29] associated with the SBA-15 existent in the sample.

Fig. 2 shows the pore diameter distributions for the supports, in all cases one can see very narrow distributions in which the variation in the pore size does not exceed 20 Å (2 nm). In the case of SBA-15, the distribution is centered at 58.9 Å (5.89 nm), while the SBA-16 shows a narrower distribution centered at 34.9 Å (3.49 nm). In the same figure it highlights the fact that the mechanical mixture of the two materials produces a bimodal pore diameter distribution with maxima at 35.8 Å (3.58 nm) and 56.4 Å (3.58 nm), which correspond with the maxima of the individual distributions for SBA-15 and SBA-16, moreover they preserve the same relative ratio of height with respect to the pure silicas.

The nitrogen adsorption–desorption isotherms and pore diameter distributions for the oxide-state and sulfided catalysts (not showed) have the same tendency and shape that those for the supports, being indicative that the porous morphology of the materials is preserved through the synthesis process; only with low displacements to lower relative pressures related with the decreasing of the pore diameter associated with the deposition of the precursors and active phases over the silicas surface onto the pores.

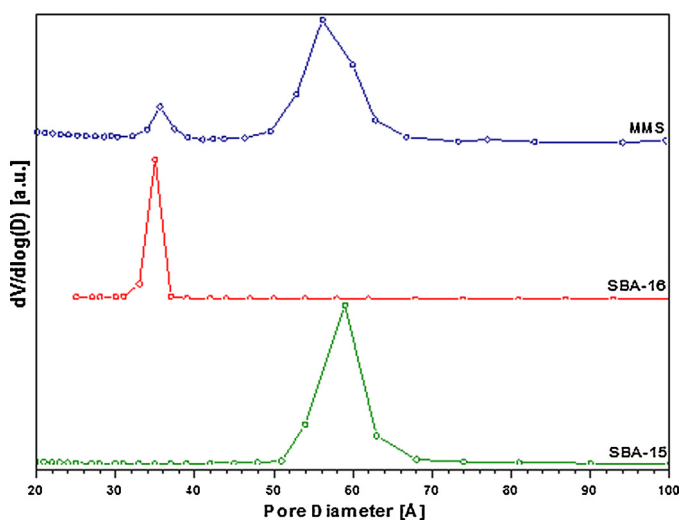


Fig. 2. Pore diameter distribution for synthesized supports (MMS – mechanical mixture of mesoporous silicas).

Table 1

Textural properties for the synthesized catalysts.

	Surface area (m^2/g)			Pore diameter (nm)			Pore volume (cm^3/g)		
	Support	Oxide state	Sulfided	Support	Oxide state	Sulfided	Support	Oxide state	Sulfided
S15ICS	819	447	235	4.788	3.415	3.404	0.897	0.464	0.327
S16ICS	462	342	106	3.413	3.409	3.055	0.275	0.134	0.040
MMICS	771	355	116	4.126*	3.411*	3.402*	0.504	0.256	0.182
IMMCS	402	169		3.422*	3.400*		0.309	0.256	
ICMMS	386	105		3.419*	3.406*		0.277		0.154

* It refers an average pore diameter for the statistical distribution, it must be remained that the distribution is bimodal and has two media (S15ICS: sulfided catalyst supported in SBA-15, S16ICS: sulfided catalyst supported in SBA-16, MMICS: sulfided catalyst supported on mixed silicas following the route mechanical mixture – impregnation – calcination – sulfidation, IMMCS: sulfided catalyst supported on mixed silicas following the route impregnation – mechanical mixture – calcination – sulfidation, ICMMS: sulfided catalyst supported on mixed silicas following the route impregnation – calcination – mechanical mixture – sulfidation).

The textural properties of the synthesized catalysts are summarized in the Table 1, in the table the samples are referred to the sulfided catalysts and the Support and Oxide-State columns refer to the properties of the materials previous to sulfidation; it is possible to observe that the pure SBA materials have large surface areas suitable for their use as catalyst supports, while the samples prepared by mechanical mixing of these materials provide intermediate values for the area, volume and pore diameter, as expected; however, the effect on the values of these parameters appears not to be linearly related to the amount of each material in the mixture (50–50%). In the same Table it can be appreciated a drastic reduction in surface area after impregnation and calcination steps (Oxide-State column), between 50 and 60%, related with the deposition and formation of the oxide precursors of the active phases; and after sulfidation the reduction is almost 80–90% respect to the original support surface area, which is indicative of the high dispersion of the active phases on the support and the possible formation of clusters of oxides of transition metals which occlude smaller pores; this effect is greater in the catalysts supported in pure SBA-16 (S16ICS) because of its smaller pores dimension.

3.2. Small-angle X-ray diffraction

X-ray diffractograms obtained at small angles for the mesoporous silica supports are shown in Fig. 3. The presence of defined peaks in all samples is evidence of the existence of well-structured mesoporous phases. It can be seen in the Fig. 3 that the SBA-15 shows peaks corresponding to the reflections (1 0 0), (1 1 0) and (2 0 0) of a 2D hexagonal array with space group P6mm, themselves already have been widely reported for SBA-15 [20,30,31]. Meanwhile, SBA-16 also shows the peaks corresponding to the reflections

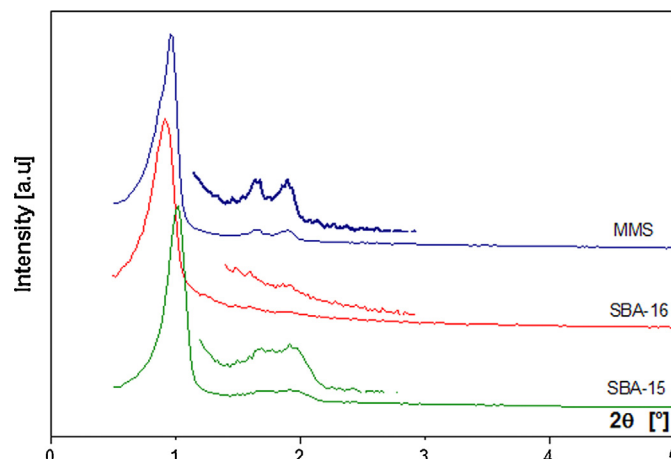


Fig. 3. Small-angle X-ray diffractograms for synthesized silica supports, for each of them is showed an amplification of the diffractogram in the range of 1–3° for 2θ (MMS – mechanical mixture of mesoporous silicas).

(1 1 0), (2 1 1) and (2 2 0) present in an Im3m cubic structure, which have also already extensively characterized in the literature [20,31]. Meanwhile, the mixture of silicas made mechanically shows a very strong peak corresponding to the reflection (1 0 0) of SBA-15, a shoulder corresponding to the (1 1 0) reflection of the SBA-16, which are accompanied by other peaks related with both mesoporous phases, confirming the incorporation of both materials in the mixture.

3.3. Wide-angle X-ray diffraction

Wide-angle diffractograms obtained for mesoporous silica supports show, in all the cases, a very broad peak centered around 24° (in a 2θ scale) corresponding to amorphous silica, which has been widely reported in numerous previous studies [4,6,20], this peak still appears in the oxide state and fresh sulfided catalysts as showed in the Figs. 4 and 5. Fig. 4 shows diffractograms for the oxide-state supported catalysts, in all of them the presence of low intensity peaks at angles 2θ of 19.5, 25, 28, 32.5, 38, 43, 28,

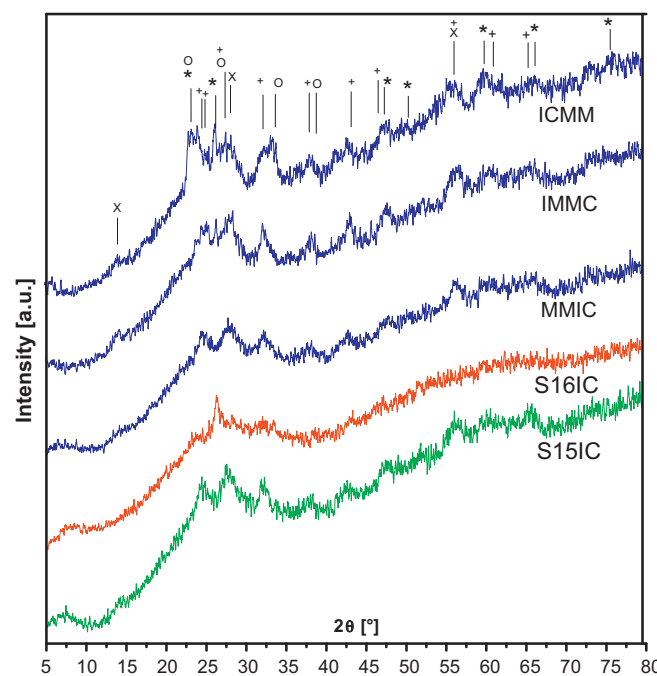


Fig. 4. Wide-angle X-ray diffractograms for oxide-state catalysts and the main identified crystalline phases: o – MoO_3 , x – WO_3 , + – $\text{CoMo(W)}\text{O}_4$, * – $\text{Mo}_x\text{W}_{1-x}\text{O}_3$. (S15IC: oxide-state catalyst supported on SBA-15, S16IC: oxide-state catalyst supported on SBA-16, MMIC: oxide-state catalyst supported on mixed silicas following the route mechanical-mixture – impregnation – calcination, IMMC: oxide-state catalyst supported on mixed silicas following the route impregnation – mechanical mixture – calcination, ICMM: oxide-state catalyst supported on mixed silicas following the route impregnation – calcination – mechanical mixture).

57 and 59.5° has been identified, corresponding to β -CoMo(W)O₄ (JCPDS-ICDD 21-0868, 15-0867), additionally with peaks corresponding to the isolated species MoO₃ (JCPDS-ICDD-76-1003) and WO₃ (JCPDS-ICDD-852460), which occurrence has already been previously reported in many studies of hydrodesulfurization catalysts containing cobalt, molybdenum and tungsten and which have been documented as precursor phases of active sites for catalysis [2–5,32]. Very low intensity peaks (not shown in the figure) has been recognized relative to the presence of oxide species of molybdenum and tungsten with formula Mo_xW_{1-x}O₃ (JCPDS-ICDD 28-0668) as well as polymolybdates and polytungstates corresponding to compounds containing large number of atoms of molybdenum and tungsten, in which the metal/oxygen ratio is between 2.75 and 2.9, as in the case of compounds such as Mo₄O₁₁, Mo₁₇O₄₇, Mo₉O₂₆, W₂₄O₆₈, W₁₇O₄₇, W₂₀O₅₈, W₁₉O₅₅, which have coordination structures similar to those of Mo(W)O₃. The low intensity of peaks in all samples is indicative that most species are widely dispersed on the surface of the supports and the presence of not well-defined peaks is due to supported species that are amorphous or have crystallite sizes below the detection limit of the technique (<4 nm).

Fresh sulfided catalysts diffractograms are shown in Fig. 5; in all of them characteristic peaks corresponding to disulfides of molybdenum and tungsten (MoS₂, JCPDS-ICDD 75-1539; WS₂, JCPDS-ICDD 08-0237) have been identified, those with hexagonal structure which have been extensively documented as catalytic species in hydrodesulfurization [2–5,32]; it shows differences in the strength of the signals due to the degree of dispersion of the sulfides in the supports surface. The presence of broad peaks in all samples is indicative of the presence of crystalline domains of different sizes supported on mesoporous silicas. Additionally, characteristic peaks have been recognized corresponding to cobalt sulfided species in the form of Co₉S₈ (JCPDS-ICDD 02-1459) and Co_{1.62}Mo₆S₈ (JCPDS-ICDD 30-0450), which has also been documented as active species in the study of hydrodesulfurization catalysts containing molybdenum and cobalt [32], these peaks have low intensity and they suggest the formation of sulfided molybdenum and tungsten species doped with cobalt. The crystallite

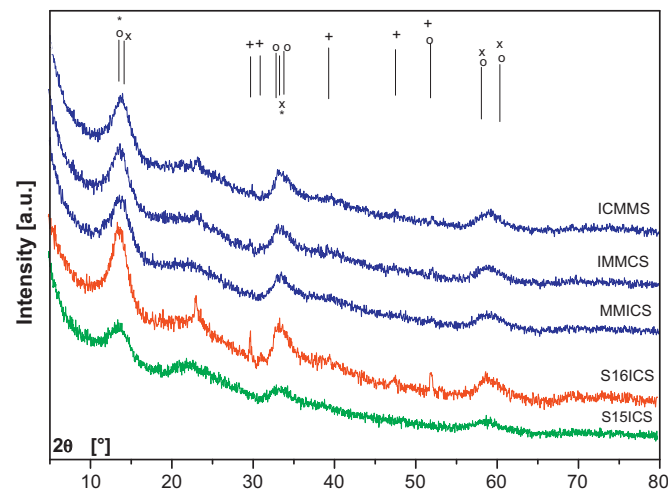


Fig. 5. Wide-angle X-ray diffractograms for fresh sulfided catalysts and the crystalline phases identified o – MoS₂, x – WS₂, + – Co₉S₈, * – Co_{1.62}Mo₆S₈, (S15ICS: sulfided catalyst supported on SBA-15, S16ICS: sulfided catalyst supported on SBA-16, MMICS: sulfided catalyst supported on mixed silicas following the route mechanical-mixture – impregnation – calcination – sulfidation, IMMCS: sulfided catalyst supported on mixed silicas following the route impregnation – mechanical mixture – calcination – sulfidation, ICMMS: sulfided catalyst supported on mixed silicas following the route impregnation – calcination – mechanical mixture – sulfidation).

sizes for the Mo(W)S₂ were determined as 28–31 Å for all the samples with the PDLX software Version 2.3.1.0 by Rigaku®, using the Williamson–Hall method.

3.4. Scanning electron microscopy

Morphology of the synthesized materials has been studied by scanning electron microscopy. SBA-15 and catalysts supported over it show the typical morphology associated with this material consisting of particles in the form of rollers or bars of about 1 µm aggregated in long tubular clusters of several microns long [20,31,33]. SBA-16 and the catalyst supported over it present typical morphology [21,34] comprising spherical particles of about 0.5 µm aggregated in clusters with dimension between 10 and 50 µm; that morphology is retained during all the synthesis process and in the case of SBA-16-supported catalysts it can be seen the presence of sintered particles generated during the calcination of the material in the different steps of the catalysts preparation. The corresponding images for the sulfided catalyst can be seen in the Fig. 6A and B.

Meanwhile, the catalysts supported on mixtures of silicas made mechanically show the same morphology of the pure supports, therein it can be seen that the incorporation of the two phases is only physical and the subsequent steps of the preparation do not cause significant changes in the morphology and average size of the materials particles. Small differences in the dispersion and incorporation of the SBA-15 and SBA-16 in the mixtures derived from the different sequences used for make the mixture can be seen, IMMCS sample (Impregnated + Mechanically Mixed + Calcined + Sulfided, Fig. 6D) has showed a greater dispersion and incorporation of the support phases, resulting in a better preservation of the morphological properties of the initial materials and a minor sintering effect of the SBA-16 particles. MMICS sample (Mechanically Mixed + Impregnated + Calcined + Sulfided, Fig. 6C) showed little differences in morphology compared with the catalysts supported in the pure silica materials. ICMMS catalyst (Impregnated + Calcined + Mechanically Mixed + Sulfided, Fig. 6E) has shown the presence of greater quantity of SBA-16 sintered particles than the other samples and a greater size of the sintered domains, between 10 and 100 µm.

3.5. Chemical analysis

Chemical analysis of the catalysts was made by energy dispersive spectroscopy (EDS). Spectra for oxide-state catalyst (not presented) have shown the presence of characteristic signals corresponding to the electronic transitions of the expected elements in the samples (O, Si, Mo, Co and W); the absence of the signal corresponding to carbon is indicative of complete removal of the polymeric surfactant used as directing agent for the synthesis of mesostructured materials. Fresh sulfided catalysts spectra show the same signals, in addition to those corresponding to sulfur electronic transitions.

By this technique, semiquantitative elemental composition of the samples can be determined which is reported in Table 2. It can be noted that the values determined experimentally are close to those established theoretically (from the calculated atomic ratios proposed in the synthesis), which is evidence of the homogeneity in the distribution of the metals transition in the samples, and the effectiveness of the impregnation method used for the synthesis of catalysts with homogeneous distribution of the active species. In this table it can be also observed that the chemical composition is similar for all the catalysts and the differences between samples are into the range of the experimental error of the analytical technique so it can be assumed a similar metal charge in all the catalysts.

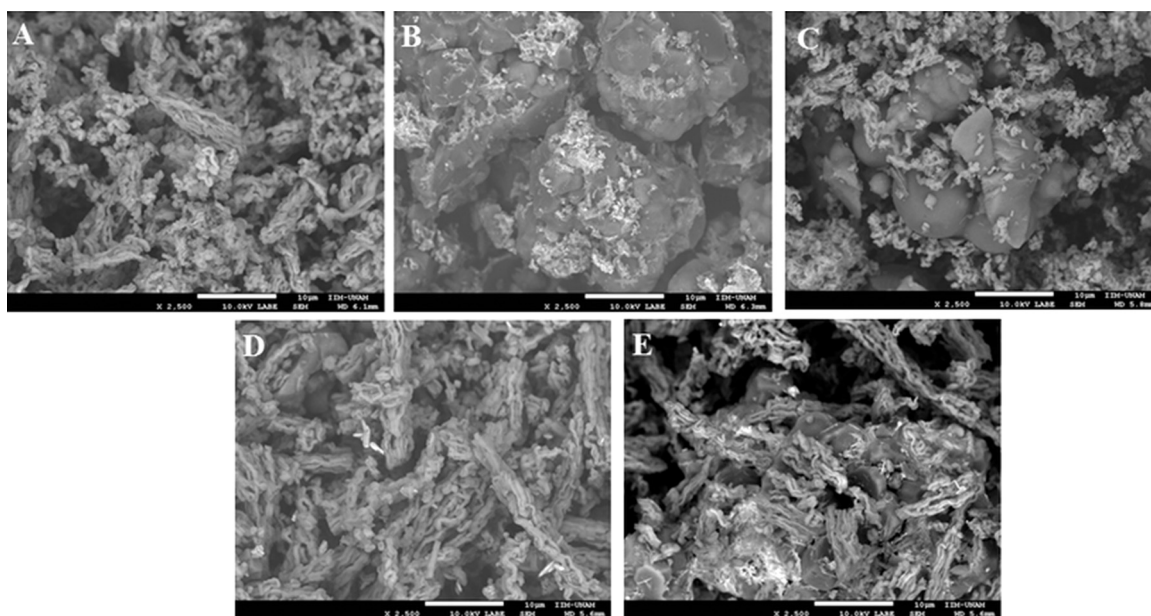


Fig. 6. Scanning electron microscopy images obtained for the fresh sulfided catalysts (A-S15ICs: sulfided catalyst supported on SBA-15, B-S16ICs: sulfided catalyst supported on SBA-16, C-MMICS: sulfided catalyst supported on mixed silicas following the route mechanical-mixture – impregnation – calcination – sulfidation, D-IMMCS: sulfided catalyst supported on mixed silicas following the route impregnation – mechanical mixture – calcination – sulfidation, E-ICMMS: sulfided catalyst supported on mixed silicas following the route impregnation – calcination – mechanical mixture – sulfidation), in all the cases it can be seen preservation of the morphological properties along the synthesis process and sintering effects in the SBA-16 domains.

Fig. 7 reproduces the elemental mapping images obtained for the most active sulfided catalyst (IMMCS: Impregnated + Mechanically Mixed + Calcined + Sulfided), similar results have been obtained for all the samples. It can be observed a homogeneous distribution of the transition metals and sulfur over the sample surface, which is indicative of a high dispersion of active phases on the surface of the catalysts. In such maps, also is evident the similarity of the distribution obtained for molybdenum and sulfur, suggesting that used sulfurization process for the catalysts synthesis allows the complete transformation of the oxides deposited on the support and a high dispersion of disulfide species.

3.6. High-resolution transmission electron microscopy

High-resolution transmission electron microscopy (HRTEM) micrographs of supports are showed in **Fig. 8**. Concerning the support morphology, HRTEM images confirmed the regular porous arrangement of the SBA-15- and SBA-16-supported catalysts. **Fig. 8A** shows mesoporous silicas mechanically mixed before impregnation. It can be observed the presence of the typical channels of the SBA-15 hexagonal structure as well as a zone with the characteristic cubic *Im3m* structure of the SBA-16 along the [100] direction. In **Fig. 8B** a Z-contrast image of fresh sulfided IMMCS

(Impregnated + Mechanically Mixed + Calcined + Sulfided) catalyst is showed, in which the contrast is associated with the atomic number of the atoms in the sample, such that the more brilliant zones indicate the presence of elements with higher atomic number. Thus, the support mesoporous structure is observed as well as the distribution of the active phases onto the pore channels forming clusters of nanoparticles, observed as brilliant dots in the image. In other words, this Z-contrast image reveals that the active phases Mo(W)S₂ are well dispersed over the support, both on the surface as well as inside the pores. This is consistent with EDS and textural results, and explains the reduction of pore diameter and surface area reported in nitrogen adsorption-desorption studies.

Fig. 9A shows an HRTEM micrograph of fresh sulfided IMMCS catalyst. The presence of two crystalline structures is observed, corresponding to MoS₂ and Co₉S₈ as identified in **Fig. 9A** and B, respectively, which are segregated from a continuous crystalline phase suggesting the presence of Mo(W)S₂ phases doped with cobalt which have been documented as active sites responsible of catalysis for hydrodesulfurization [35,36,63]. An interplanar distance d_{004} of 3.13 Å, corresponding to (004) planes of molybdenum disulfide structure, was determined in **Fig. 9B**. Even if MoS₂ fringes appear regularly stacked, their organization is relatively disordered. **Fig. 9C** was obtained by performing a Fast Fourier Transform (FFT) to the square marked in **Fig. 9A**. Bragg diffraction

Table 2

Elemental composition of the oxide-state catalysts obtained by EDS.

Sample*	O	Si	Co	Mo	W	Co/(Mo + W)	Mo/(Mo + W)	W/(Mo + W)
Expected	67.22	28.81	1.19	1.39	1.39	0.43	0.5	0.5
S15IC	71.13	24.54	1.12	2.07	1.16	0.35	0.64	0.36
S16IC	69.77	26.32	1.23	1.44	1.26	0.46	0.53	0.47
MMIC	70.07	25.22	1.14	1.66	1.92	0.32	0.46	0.54
IMMC	70.76	24.88	1.11	1.58	1.74	0.33	0.48	0.52
ICMM	70.77	25.21	1.12	1.38	1.54	0.38	0.47	0.53

* S15IC: oxide-state catalyst supported on SBA-15, S16IC: oxide-state catalyst supported on SBA-16, MMIC: oxide-state catalyst supported on mixed silicas following the route mechanical-mixture – impregnation – calcination, IMMC: oxide-state catalyst supported on mixed silicas following the route impregnation – mechanical mixture – calcination, ICMM: oxide-state catalyst supported on mixed silicas following the route impregnation – calcination – mechanical mixture.

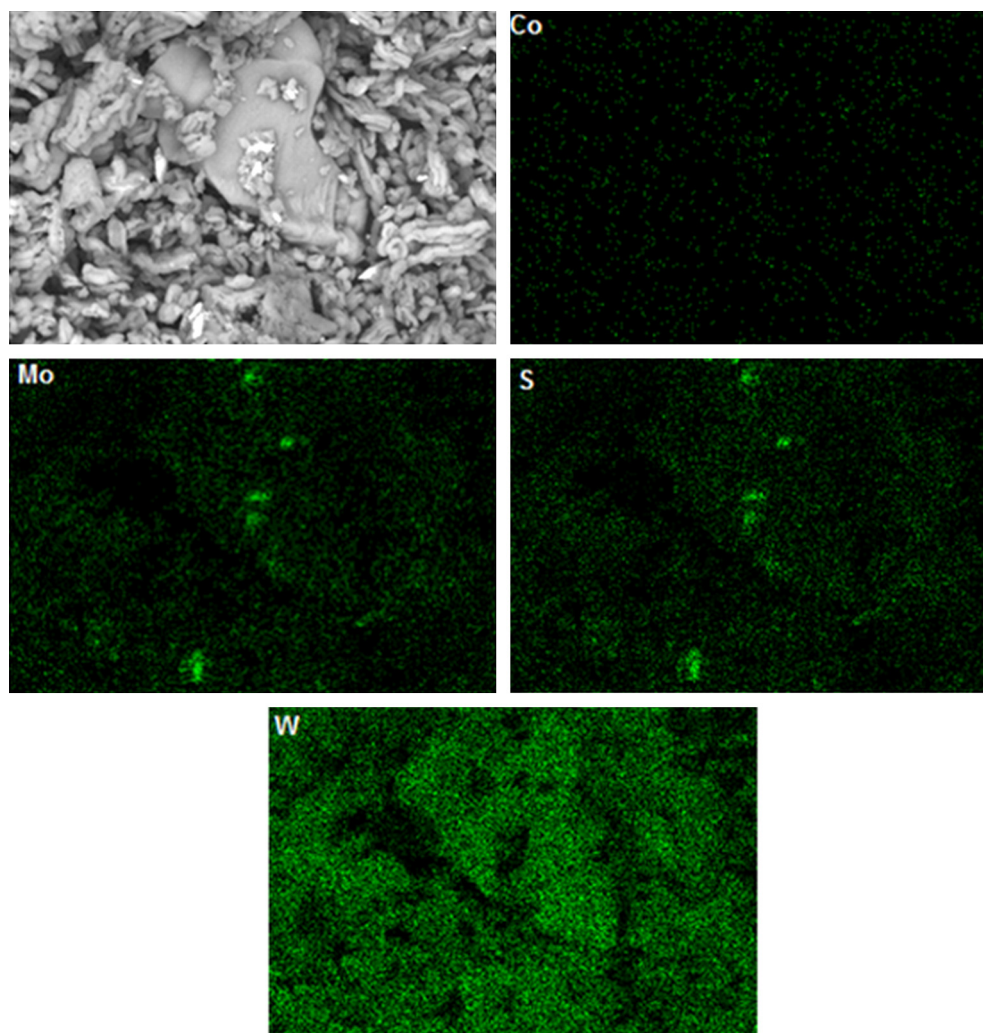


Fig. 7. Elemental distribution obtained by EDS for the IMMCS catalyst (Impregnated + Mechanically Mixed + Calcined + Sulfided).

reflections, corresponding to (111), (200) and (220) planes of Co_9S_8 structure were identified. These results are in agreement with those obtained in the XRD analysis, and the presence of these two phases is important for the catalytic activity [35,36], as will be discussed later.

3.7. DRS-UV-vis spectroscopy

The diffuse reflectance spectra in the UV-visible range for the oxide state catalysts are presented in Fig. 10 accompanied with the corresponding deconvolution peaks obtained with a mathematical

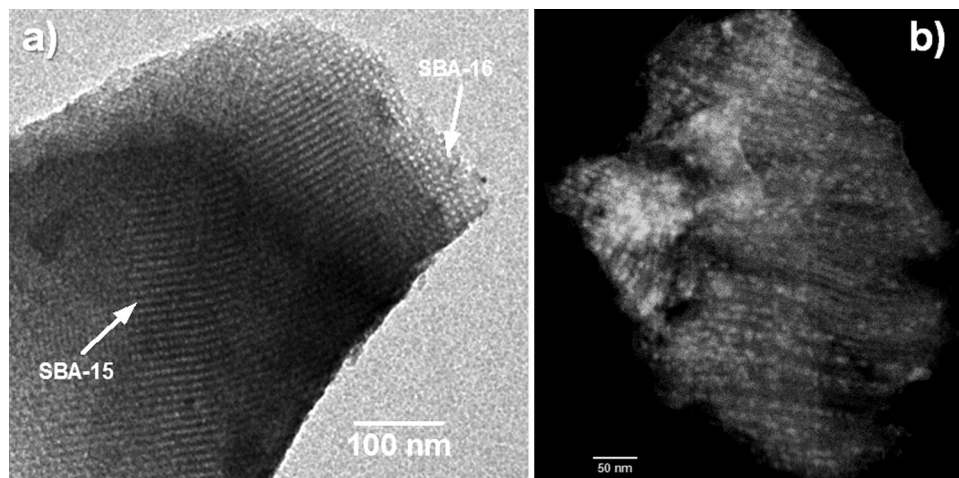


Fig. 8. HRTEM micrographs of mesoporous silicas mechanically mixed before impregnation (A) and Z-contrast image of fresh sulfided IMMCS catalyst (Impregnated – mechanically mixed – calcined – sulfided) (B).

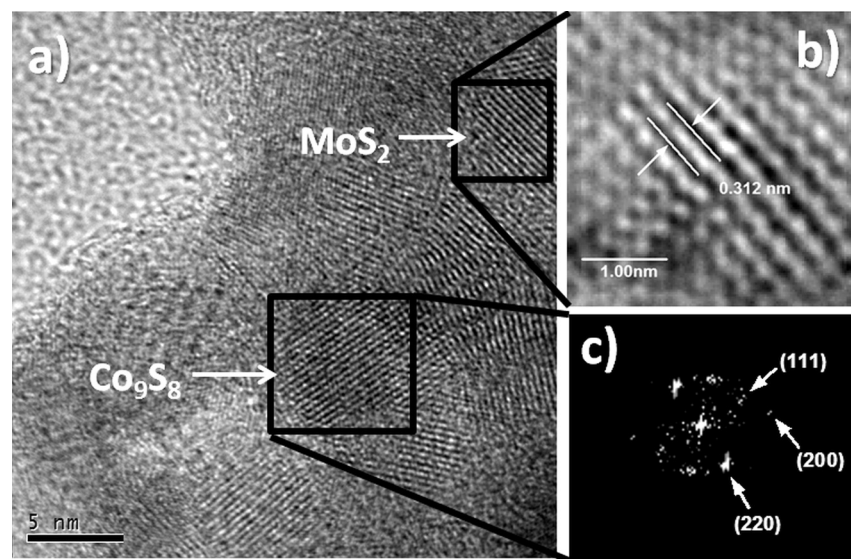


Fig. 9. HRTEM image of IMMC catalyst [Impregnated + Mechanically Mixed + Calcined + Sulfided] (A), zoom on typical MoS₂ slabs (B) and FFT of the square marked indicating the Bragg reflections of (1 1 1), (2 0 0) and (2 2 0) of planes of Co₉S₈ (C).

software using Gaussian functions. In all the spectra a very intense band between 200 and 350 nm has been identified which deconvolution denotes the presence of three closer bands: a band between 220 and 240 nm corresponding to the ligant-metal charge transfer related to the presence of Mo⁶⁺ and W⁶⁺ ions in tetrahedral coordination like in WO₄²⁻ and MoO₄²⁻ isolated species, whose presence on silica supported catalysts has already been reported [4–6,37]; a second band at 290–300 nm has been attributed by Jeziorowski et al. [38,39] to ligant-metal charge transfer transitions in Mo–O–Mo bonds present in octahedral polymolybdates, while that at 320–340 nm has been reported as the corresponding to the ligant-metal charge transfer transition from the O²⁻ to Mo⁶⁺(W⁶⁺) in octahedral coordination compounds such as polymolybdates and polytungstates [4–6,40,41]; both types of compounds were identified in the analysis of wide-X-ray diffraction, so these results are consistent with the fact that the structure of the species supported on environmental conditions is governed by the acid-base interactions between transition metals and the support, so that the silica having an acidic surface tends to form species which are stable under acidic conditions, such as Mo₇O₂₆⁴⁻ and Mo₈O₂₄⁶⁻ [32,38,42–44].

The presence of broad bands indicates that the metal oxides are present in aggregates of different sizes. In all samples a similar amount of octahedral molybdenum and tungsten species is observed, except for the IMMC (Impregnated + Mechanically Mixed + Calcined) which shows a higher band corresponding to these species, similar results were obtained for the content of species in tetrahedral coordination, which shows that in this catalyst metal-support interactions are more significant.

Concerning the band at 500–520 nm, it has been previously reported as corresponding to charge transitions in Co²⁺ complexes with octahedral coordination [45], and the band observed between 565 and 580 nm has been attributed in previous studies to the d-d electronic transitions (4T_{2g} to 4A_{2g} and 4T_{2g} to 4T_{1g}) in octahedral high spin cobalt complexes present in the β-CoMoO₄, in which the cobalt is interacting with molybdenum and whose presence already been identified by X-ray diffraction; this octahedral ion has been observed to be easily sulfided to generate active species for catalytic hydrodesulfurization reactions [4–6,46]; however, in this range the occurrence of charge transfer transitions for Co²⁺ species in tetrahedral coordination also has been reported [47], that is indicative of the presence of cobalt ions interacting directly with the support

as Co₂SiO₄, this suggests the presence of small amounts of these species supported on the catalysts.

3.8. Micro Raman spectroscopy

Micro Raman spectra obtained for the oxide-state catalysts are shown in Fig. 11; it can be appreciated that all of them show a very intense band in the range of 900–1000 cm⁻¹, whose position and intensity is indicative of the presence of several species of tungsten and molybdenum with different symmetries. Deconvolution of this band was done using a mathematical software and based on Gaussian functions (not shown), in the deconvolution a strong peak at 940–960 cm⁻¹ can be seen and it is attributed to the symmetric stretching vibration of the terminal bond Mo(W)=O in various types of polymolybdates and polytungstates with octahedral coordination of the metal, whose intensity is enriched by the contribution of the Si–O stretching of the silanol groups present in silica which appears in the same range. Additionally, it is present a very low intense band at 980–985 cm⁻¹ and a low intensity band near to 860 cm⁻¹ which have been reported as corresponding to the O–Mo–Mo–O stretching vibrations of distorted polymolybdates [41,48,49]. Polytungstates presence in samples is confirmed by the appearance of a low intensity bands at 510 cm⁻¹ and 200–300 cm⁻¹ corresponding to stretching and angular deformation of the W–O–W bonds, respectively [40,50,51]. Dioxo compounds of molybdenum and tungsten are presented as isolated species with tetrahedral coordination which is evidenced by the appearance of an intense band at 970–975 cm⁻¹ corresponding to the asymmetric stretching of the O=Mo(W)=O bonds and a contribution to the band at 990–995 related to the symmetric stretching of O=Mo(W)=O bonds [40,50]. The presence of an intense band between 935 and 945 cm⁻¹ may be ascribed as the W=O symmetrical stretching related with tungsten in tetrahedral position such as in WO₄²⁻ ion, which is presented in isolated species of CoWO₄. The presence of this compound in the catalysts is confirmed by the appearance of a low intensity band at 730–740 cm⁻¹ attributed to the O–W–O asymmetrical vibration [37,40]. The displacement of this band is indicative of distortion in the tetrahedral structure of the complex. The presence of molybdenum species isolated in tetrahedral coordination, as β-CoMoO₄, is assumed by the presence in all samples of the bands at 890–900 cm⁻¹ corresponding to the Mo–Co–O stretching vibration,

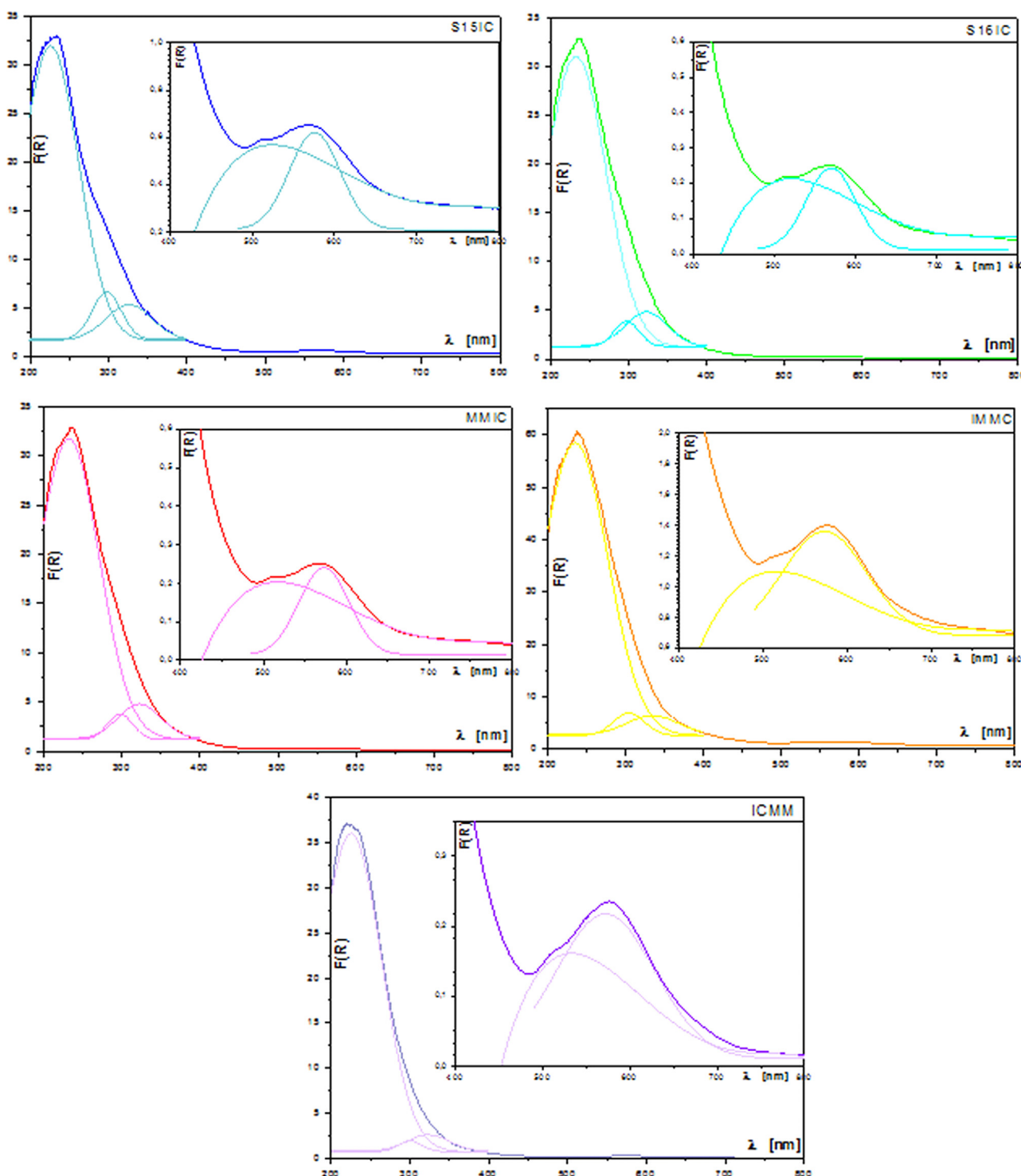


Fig. 10. Diffuse reflectance UV-vis spectra for the oxide-state catalysts and their deconvolution in Gaussian functions (S15IC: oxide-state catalyst supported on SBA-15, S16IC: oxide-state catalyst supported on SBA-16, MMIC: oxide-state catalyst supported on mixed silicas following the route mechanical-mixture – impregnation – calcination, IMMC: oxide-state catalyst supported on mixed silicas following the route impregnation – mechanical mixture – calcination, ICMM: oxide-state catalyst supported on mixed silicas following the route impregnation – calcination – mechanical mixture).

at $830\text{--}840\text{ cm}^{-1}$ associated with Mo–O asymmetric stretching and at 317 cm^{-1} related to the O–Mo–O angular deformation [52].

The presence of bands at $990\text{--}995$ and $815\text{--}820\text{ cm}^{-1}$, in addition to low intensity bands at $708, 666, 417, 377, 338, 290, 248, 217, 198$ and 160 cm^{-1} are signals of the presence of MoO_3 supported on silica as has been reported previously [41]; low intensity bands are

observed in all spectra at 715 cm^{-1} and 435 cm^{-1} associated with WO_3 . Most of the samples exhibit bands at $990, 970$ and 910 cm^{-1} , which appear as masked signals on the main band, additionally to low intensity bands at $635, 252$ and 220 cm^{-1} , which have been previously reported as corresponding to silico-molybdic anion $[\text{SiMo}_{12}\text{O}_{40}]^{4-}$ [53]. It can be seen a very low intensity band around

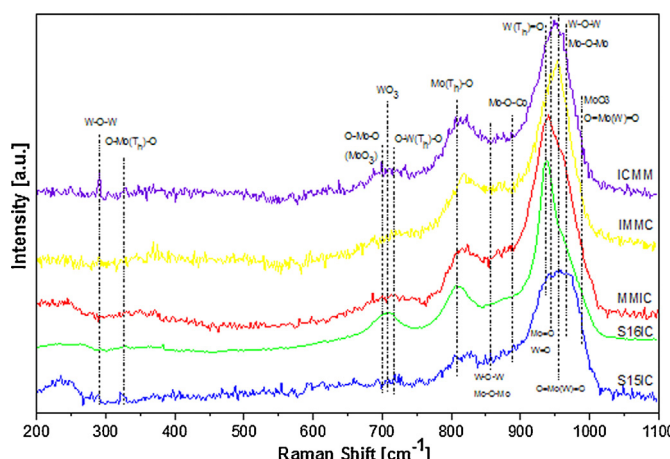


Fig. 11. Micro Raman spectra for the oxide-state catalysts functions (S15IC: oxide-state catalyst supported on SBA-15, S16IC: oxide-state catalyst supported on SBA-16, MMIC: oxide-state catalyst supported on mixed silicas following the route mechanical-mixture – impregnation – calcination, IMMC: oxide-state catalyst supported on mixed silicas following the route impregnation – mechanical mixture – calcination, ICMM: oxide-state catalyst supported on mixed silicas following the route impregnation – calcination – mechanical mixture).

1020 cm⁻¹ associated with the stretching vibration of the Mo=O bond in mono-oxided molybdenum species attached directly to the support [41].

Table 3 shows the values calculated for the ratio of metal–oxygen terminal bonds [Mo(W)=O] and metal–oxygen bulk bonds [Mo(W)–O–Mo(W)], obtained from the deconvolution peak areas of the bands at 950–960 cm⁻¹ and 980–985 cm⁻¹; the value of this ratio is very important in catalytic hydrodesulfurization reactions since previous studies have shown the influence of the presence of terminal metal–oxygen bonds in the formation of catalytic sites [54]. In the table it can be seen that the values of this ratio are higher for catalysts supported on two of the mechanical mixture of silicas, coinciding with the results for catalytic activity (measured as apparent reaction rate constant value and discussed in the next section), showing that there is a close correlation between the presence of terminal bonds and catalytic activity.

3.9. Catalytic performance

The catalytic activity of the synthesized materials in the hydrodesulfurization reaction (HDS) of dibenzothiophene (DBT) was measured using the apparent rate constant calculated by the method described in the Experimental section. In Fig. 12 the dibenzothiophene conversion profiles are shown, as was experimentally determined; it can be seen that all catalysts follow an exponential behavior, as is expected for this type of chemical reactions

Table 3

Relation between terminal and bulk metal–oxygen bonds for the oxide-state catalysts.

Catalyst*	Mo(W)=O/O-Mo(W)-O ratio
S15IC	1.13
S16IC	2.77
MMIC	4.37
IMMC	6.66
ICMM	0.79

* (S15IC: oxide-state catalyst supported on SBA-15, S16IC: oxide-state catalyst supported on SBA-16, MMIC: oxide-state catalyst supported on mixed silicas following the route mechanical-mixture – impregnation – calcination, IMMC: oxide-state catalyst supported on mixed silicas following the route impregnation – mechanical mixture – calcination, ICMM: oxide-state catalyst supported on mixed silicas following the route impregnation – calcination – mechanical mixture).

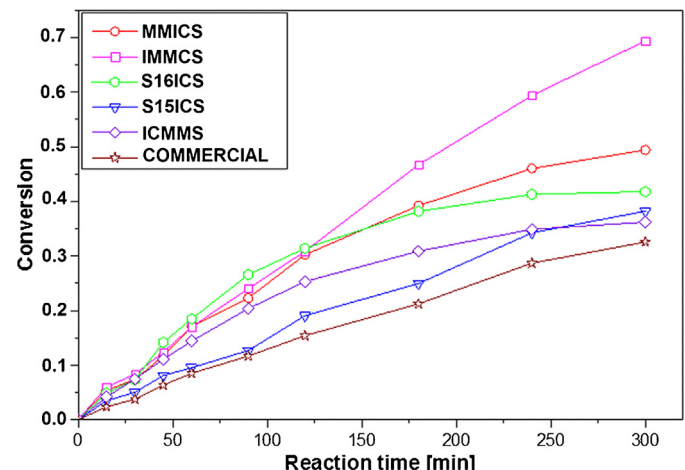


Fig. 12. Conversion profile for the hydrodesulfurization reaction of DBT for the synthesized catalysts and the commercial one used as comparative model (S15ICS: sulfided catalyst supported on SBA-15, S16ICS: sulfided catalyst supported on SBA-16, MMICS: sulfided catalyst supported on mixed silicas following the route mechanical-mixture – impregnation – sulfidation, IMMCS: sulfided catalyst supported on mixed silicas following the route impregnation – mechanical mixture – sulfidation, ICMMS: sulfided catalyst supported on mixed silicas following the route impregnation – calcination – mechanical mixture – sulfidation).

according to the pseudo-first order model proposed. The graph shows that before 120 min of reaction, the conversion profile has a linear behavior for all the catalysts as expected from the pseudo-first order model proposed suggesting that in this step the rate is controlled only for the kinetics of the reaction [19,22–25,55], after that time they become important the diffusive and mass transfer effects in the reaction system and the presence of collateral reversible reactions. In this figure it can be seen that two of the catalysts supported on silicas mechanical mixtures, the IMMCS and MMICS, show a greater degree of conversion of dibenzothiophene throughout the reaction time over those supported on pure SBA-15 and SBA-16 and even the commercial catalyst used as reference, while the catalyst ICMMS has a lower catalytic behavior.

The values obtained for the apparent rate constant for the tested catalysts are shown in Table 4, these values were obtained from the time and conversion data using a linear regression in which the regression coefficient (R^2) took values between 0.982 and 0.999 for the different samples and the standard error for the values of apparent rate constants were between 3 and 5%. The fact that an equal mass of catalyst was used for every experiment and that all of them have similar metal charge (as determined by the EDS results) allows to take this parameter as comparative element for the catalytic activity of the samples; it can be seen that two of the catalysts supported on mixtures of mesoporous silica (IMMCS and MMICS) exhibit the highest activity in the series of synthesized catalysts, in which the difference between the values is higher than the experimental error (5%), indicating that the use of mixtures of mesoporous silica as support material is advantageous for the preparation of catalysts based on metal transition sulfides for hydrodesulfurization, in addition to the fact that the sequence of preparation (mixing impregnation-calcination) has an effect on the catalytic properties of the synthesized material.

The observed behavior is related to a higher density of sulfides of molybdenum and tungsten formed on the surface of the catalyst in the more active catalysts, as established by the results of X-ray diffraction, in which corresponding peaks are more intense for samples with higher catalytic activity and this is confirmed with the diffuse reflectance spectroscopy results, in which the more active catalysts contain a greater quantity of tetrahedral and

Table 4

Catalytic apparent constant and selectivity values (determined at 30% conversion) for the synthesized catalysts.

Catalyst*	k_{app} [mol/g _{cat} s] ($\pm 5\%$ std error)	BF [mol] ^{**}	CHB [mol] ^{**}	BCH [mol] ^{**}	DSD [mol] ^{**}	HYD [mol] ^{**}	HYD/DDS Ratio (Selectivity)
S15ICS	6.7×10^{-7}	109.79	14.54	0.00	109.79	14.54	0.13
S16ICS	8.1×10^{-7}	114.66	9.83	6.21	114.66	16.03	0.14
MMICS	8.2×10^{-7}	110.70	13.34	0.96	110.70	14.30	0.13
IMMCS	9.2×10^{-7}	117.80	13.25	0.00	117.80	13.25	0.11
ICMMS	3.4×10^{-7}	117.93	11.54	3.32	117.93	14.86	0.13
COMMERCIAL	4.7×10^{-7}	138.00	4.00	48.00	138.00	52.00	0.38

* (S15ICS: sulfided catalyst supported on SBA-15, S16ICS: sulfided catalyst supported on SBA-16, MMICS: sulfided catalyst supported on mixed silicas following the route mechanical-mixture – impregnation – calcination – sulfidation, IMMCS: sulfided catalyst supported on mixed silicas following the route impregnation – mechanical mixture – calcination – sulfidation, ICMMS: sulfided catalyst supported on mixed silicas following the route impregnation – calcination – mechanical mixture – sulfidation).

** (BF: biphenyl, CHB: cyclohexylbenzene, BCH: bicyclohexyl, DDS: direct desulfurization products, HYD: hydrogenation products).

octahedral molybdenum and tungsten species (derived from the higher area for both deconvoluted spectral bands), being known that an increase in octahedral species of these metals improves catalytic activity. It has also found in all samples the presence of oxide precursors with cobalt ions with octahedral coordination, which are beneficial in the formation of active sites for catalysis of reactions of hydrodesulfurization [54,56–62]. Additionally, the results of Micro Raman spectroscopy indicates the presence of molybdenum and tungsten species in octahedral coordination in all samples, showing a greater intensity of the bands related with this species the samples prepared by mechanical mixing of pure silicas, which is related with the fact that these catalysts contain the highest number of Mo(W)=O terminal bonds, which has been reported as responsible of the catalytic activity in the hydrodesulfurization of dibenzothiophene [54].

On the other hand, it is known that the sulfidation of CoMo(W)O₄ results in the segregation of crystals of Co₉S₈ and curved structures of Mo(W)S₂ doped with cobalt, so that the catalytic activity is the result of a “joint effect” derived from the presence of metal centers with octahedral and tetrahedral coordination, associated with particular arrangements of the active constituents [35,36,63], which are very important for adsorption, decomposition and chemical reaction of dibenzothiophene in surfaces of the catalysts [57,59,61–63], so that the most active catalysts are those that show higher concentration of both phases and were identified in the X-ray diffraction, HRTEM and spectroscopic analyses.

The other important parameter studied for the catalytic performance was the selectivity; HDS of DBT can occur by two parallel pathways: direct desulfurization (DDS) and hydrogenation (HYD); the first leads to the formation of biphenyl (BP) via hydrogenolysis, while the hydrogenation of one or two aromatic rings produces cyclohexylbenzene (CHB) and bicyclohexyl (BCH), respectively. Selectivity results for synthesized catalysts are shown in Table 4. It can be seen that all synthesized catalysts give low selectivity values, as have seen in previous studies of catalysts supported in mesoporous silicas [2–6,24,35,56,63], which implies that are highly selective to the direct desulfurization route, unlike the commercial catalyst which promotes equality both routes. Particularly, the catalysts supported on mesoporous silica mechanical mixtures give lower values with respect to those supported on pure SBA-15 and SBA-16, indicating that the use of mixtures with different mesostructure as support tends to increase the selectivity of the catalyst towards direct desulfurization route. This depletion in the hydrogenation route of DBT is related to a confinement of the sulfided active species inside the mesopores of SBA materials which hinders the adsorption of the DBT in an adequate position leading to an enhancement of the DDS selectivity [2,63]. Moreover, one of the possible routes to remove sulfur atoms from more complex molecules, such as 4,6,DMDBT, requires catalysts displaying selectivity towards hydrogenation, however, can also be the case that the route of elimination of sulfur can occur through one dealkylation

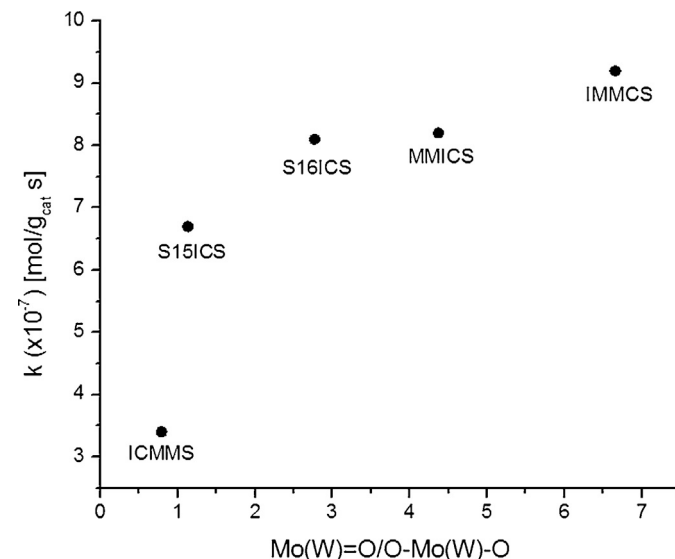


Fig. 13. Comparison between the ratio of metal–oxygen terminal bonds and catalytic performance. (S15ICS: sulfided catalyst supported on SBA-15, S16ICS: sulfided catalyst supported on SBA-16, MMICS: sulfided catalyst supported on mixed silicas following the route mechanical-mixture – impregnation – calcination – sulfidation, IMMCS: sulfided catalyst supported on mixed silicas following the route impregnation – mechanical mixture – calcination – sulfidation, ICMMS: sulfided catalyst supported on mixed silicas following the route impregnation – calcination – mechanical mixture – sulfidation).

(DA), followed by a direct desulfurization (DDS), which has been previously reported [64]. Although differences in HYD/DDS ratio values between the synthesized catalysts are small, they are above the experimental error in measured concentrations (2–3%) and it allows to assume that the difference between the samples is significant.

Fig. 13 shows a comparison between the ratio of metal–oxygen terminal bonds and catalytic performance. It can be observed that with increasing concentration of Mo(W)=O terminal bonds, the catalytic activity increases, which can be explained because there is a better sulfidation of the oxides and an increase in edge sites.

4. Conclusions

The use of mesoporous silicas mechanically mixed as support for catalytic materials show advantages over the use of such materials separately in the preparation of trimetallic catalysts based on transition metal sulphides. This improvement is attributed to the presence of different mesoporous structures, which has a positive effect over the diffusion processes of the precursors of the active phases on the support, which promotes a higher formation of desirable precursor phases, as well as due to the fact that mesoporous silicas have suitable pore dimensions for the diffusion of

the reactants and the products which inhibits the external mass transfer limitations; the whole result is a higher catalytic activity for the HDS reactions of dibenzotriphene, even more than that of the commercial catalyst used as comparative model. It has been seen that the improvement in activity is also related with the stage of the synthesis process in which the mixture is done, this suggest that the higher activity result from different levels of electronic and chemical interaction between precursors and the support material.

Acknowledgments

Authors would like to thank to CONACYT scholarship and Project DGAPA-UNAM-PAPIIT IN107311 as well as to CONACYT 182191 and CIC UMSNH 2014–2015 projects for the financial support. Also, authors acknowledge the assistance of Dr. Gabriel Alonso Nuñez and Dr. Trino Zepeda (CNyN-UNAM) in the catalytic performance measurements, Ing. Francisco Rodríguez Melgarejo (CINVESTAV-Querétaro) in the Micro-Raman Spectroscopy characterization, Dr. Rodrigo Esparza and M. Ing. Q. Alicia del Real López for their assistance in the SEM and EDS studies and Dr. Jesús Arenas Alatorre for his assistance in HRTEM analysis.

References

- [1] Annual Energy Outlook 2012 with Projections to 2035, (2012).
- [2] R. Nava, R.A. Ortega, G. Alonso, C. Ornelas, B. Pawelec, J.L.G. Fierro, *Catal. Today* 127 (2007) 70–84.
- [3] R. Nava, B. Pawelec, J. Morales, R.A. Ortega, J.L.G. Fierro, *Micropor. Mesopor. Mater.* 118 (2009) 189–201.
- [4] R. Huirache-Acuña, B. Pawelec, E.M. Rivera-Muñoz, R. Nava, J. Espino, J.L.G. Fierro, *Appl. Catal. B - Environ.* 92 (2009) 168–184.
- [5] R. Huirache-Acuña, B. Pawelec, C.V. Loricera, E.M. Rivera-Muñoz, R. Nava, B. Torres, J.L.G. Fierro, *Appl. Catal. B - Environ.* 125 (2012) 473–485.
- [6] R. Huirache-Acuña, R. Nava, C.L. Peza-Ledesma, J. Lara-Romero, G. Alonso-Núñez, B. Pawelec, E.M. Rivera-Muñoz, *Materials* 6 (2013) 4139–4167.
- [7] K. Soni, K.C. Mouli, A.K. Dalai, J. Adjaye, *Catal. Lett.* 136 (2010) 116–125.
- [8] K. Soni, T. Bhaskar, M. Kumar, K.S.R. Rao, G.M. Dhar, *ACS Symp. Ser.* 1132 (2013) 161–192.
- [9] T. Klimova, L. Lizama, J.C. Amezcua, P. Roquero, E. Terrés, J. Navarrete, J.M. Domínguez, *Catal. Today* 98 (2004) 141–150.
- [10] J.A. Mendoza-Nieto, O. Vera-Vallejo, L. Escobar-Alarcón, D. Solís-Casados, T. Klimova, *Fuel* 110 (2013) 268–277.
- [11] L. Lizama, T. Klimova, *Appl. Catal. B - Environ.* 82 (2008) 139–150.
- [12] V. Sundaramurthy, I. Eswaramoorthi, A.K. Dalai, J. Adjaye, *Micropor. Mesopor. Mater.* 111 (2008) 560–568.
- [13] P.E. Boahene, K.K. Soni, A.K. Dalai, J. Adjaye, *Appl. Catal. A - Gen.* 402 (2011) 31–40.
- [14] P. Rayo, M.S. Rana, J. Ramírez, J. Ancheyta, A. Aguilar-Elguézabal, *Catal. Today* 130 (2008) 283–291.
- [15] P. Rayo, J. Ramírez, M.S. Rana, J. Ancheyta, A. Aguilar-Elguézabal, *Ind. Eng. Chem. Res.* 48 (2009) 1242–1248.
- [16] R. Palcheva, A. Spojakina, L. Dimitrov, K. Jiratova, *Micropor. Mesopor. Mater.* 122 (2009) 128–134.
- [17] O.Y. Gutiérrez, F. Pérez, G.A. Fuentes, X. Bokhimi, T. Klimova, *Catal. Today* 130 (2008) 292–301.
- [18] A. Sampieri, S. Pronier, S. Brunet, X. Carrier, C. Louis, J. Blanchard, K. Fajerwerg, M. Breysse, *Micropor. Mesopor. Mater.* 130 (2010) 130–141.
- [19] D. Gao, A. Duan, X. Zhang, Z. Zhao, E. Hong, J. Li, H. Wang, *Appl. Catal. B - Environ.* 165 (2015) 269–284.
- [20] D. Zhao, J. Feng, Q. Huo, N. Melosh, G. Fredrickson, B. Chmelka, G.D. Stucky, *Science* 279 (1998) 548–552.
- [21] K. Flodström, V. Alfredsson, *Micropor. Mesopor. Mater.* 59 (2003) 167–176.
- [22] H. Farag, *Energ. Fuel* 20 (2006) 1815–1821.
- [23] Y. Wang, Z. Sun, A. Wang, L. Ruan, M. Lu, J. Ren, X. Li, C. Li, Y. Hu, P. Yao, *Ind. Eng. Chem. Res.* 43 (2004) 2324–2329.
- [24] G. Berhault, M. Pérez de la Rosa, A. Mehta, M.J. Yácaman, R.R. Chianelli, *Appl. Catal. A - Gen.* 345 (2008) 80–88.
- [25] J. Chen, H. Yang, Z. Ring, *Catal. Today* 98 (2004) 227–233.
- [26] T.A. Zepeda, B. Pawelec, J.N. Díaz de León, J.A. De los Reyes, A. Olivas, *Appl. Catal. B - Environ.* 111–112 (2012) 10–19.
- [27] G. Leo fanti, M. Padovan, G. Tozzola, B. Venturelli, *Catal. Today* 41 (1998) 207–219.
- [28] K. Sing, *Colloid. Surf. A* 187–188 (2001) 3–9.
- [29] K.S.W. Sing, D.H. Everett, R.A.W. Haul, L. Moscou, R.A. Pierotti, J. Rouquérol, T. Siemieniewska, *Pure Appl. Chem.* 57 (1985) 603–619.
- [30] M. Kruck, C.H. Ko, R. Ryoo, M. Jaroniec, *Chem. Mater.* 12 (2000) 1961–1968.
- [31] V. Meynen, P. Cool, E.F. Vansant, *Micropor. Mesopor. Mater.* 125 (2009) 170–223.
- [32] V. La Parola, G. Deganello, C.R. Tewell, A.M. Venezia, *Appl. Catal. A - Gen.* 235 (2002) 171–180.
- [33] E.M. Johansson, J.M. Córdoba, M. Odén, *Mater. Lett.* 63 (2009) 2129–2131.
- [34] M.A. Ballem, J.M. Córdoba, M. Odén, *Micropor. Mesopor. Mater.* 129 (2010) 106–111.
- [35] R. Huirache-Acuña, G. Alonso-Núñez, F. Paraguay-Delgado, J. Lara-Romero, G. Berhault, E.M. Rivera-Muñoz, *Catal. Today* 250 (2015) 28–37.
- [36] M. Ramos, D. Ferrer, E. Martínez-Soto, H. Lopez-Lippmann, B. Torres, G. Berhault, R.R. Chianelli, *Ultramicroscopy* 127 (2013) 64–69.
- [37] E.I. Ross-Medgaarden, I.E. Wachs, *J. Phys. Chem. C* 111 (2007) 15089–15099.
- [38] H. Jeziorski, H. Knözinger, *J. Phys. Chem.* 83 (1979) 1166–1173.
- [39] H. Jeziorski, H. Knezinger, P. Grange, P. Gajardo, *J. Phys. Chem.* 14 (1980) 1825–1829.
- [40] D.G. Barton, M. Shtain, R.D. Wilson, S.L. Soled, E. Iglesia, *J. Phys. Chem. B* 103 (1999) 630–640.
- [41] C.C. Williams, J.G. Ekerdt, J.M. Jehng, F.D. Hardcastle, A.M. Turek, I.E. Wachs, *J. Phys. Chem.* 95 (1991) 8781–8791.
- [42] J. Fournier, C. Luois, M. Che, P. Chaquin, D.J. Masure, *J. Catal.* 119 (1989) 415–425.
- [43] R.A. Schoonheydt, *Chem. Soc. Rev.* 39 (2010) 5051–5066.
- [44] J.P. Thielemann, T. Ressler, A. Walter, G. Tzolova-Müller, C. Hess, *Appl. Catal. A - Gen.* 399 (2011) 28–34.
- [45] J.D. Han, S.I. Woo, *Korean J. Chem. Eng.* 8 (1991) 235–239.
- [46] J.E. Herrera, D.E. Resasco, *J. Catal.* 221 (2004) 354–364.
- [47] A. Szegedi, M. Popova, C. Minchev, *J. Mater. Sci.* 44 (2009) 6710–6717.
- [48] F.D. Hardcastle, I.E. Wachs, *J. Raman Spectrosc.* 21 (1990) 683–691.
- [49] H. Hu, I.E. Wachs, *J. Phys. Chem.* 99 (1995) 10897–10910.
- [50] G. Busca, *J. Raman Spectrosc.* 33 (2002) 348–358.
- [51] F.D. Hardcastle, I.E. Wachs, *J. Raman Spectrosc.* 26 (1995) 397–405.
- [52] F.R. Brown, L.E. Makovsky, *Appl. Spectrosc.* 31 (1977) 44–46.
- [53] R.S. Weber, *J. Catal.* 151 (1995) 470–474.
- [54] P. Atanasova, T. Tabakova, Ch. Vladov, T. Halachev, A. Lopez-Agudo, *Appl. Catal. A - Gen.* 161 (1997) 105–119.
- [55] L.D. Schmidt, *The Engineering of Chemical Reactions*, Oxford University Press, NY, USA, 1998, pp. 21–85, Chapter 2.
- [56] G. Alonso-Núñez, J. Bocarando, R. Huirache-Acuña, L. Alvarez-Contreras, Z.D. Huang, W. Bensch, G. Berhault, J. Cruz, T.A. Zepeda, S. Fuentes, *Appl. Catal. A - Gen.* 419–420 (2012) 95–101.
- [57] S.M.A.M. Bouwens, F.B.M. van Zon, M.P. van Dijk, A.M. van der Kraan, V.H.J. de Beer, J.A.R. van Veen, D.C. Koningsberger, *J. Catal.* 146 (1994) 375–393.
- [58] D.H. Broderick, B.C. Gates, *AIChE J.* 27 (1981) 663–673.
- [59] F. Cesano, S. Bertarione, A. Piovano, G. Agostini, M.M. Rahman, E. Groppo, F. Bonino, D. Scarano, C. Lamberti, S. Bordiga, L. Montanari, L. Bonoldi, R. Millini, A. Zecchina, *Catal. Sci. Technol.* 1 (2011) 123–136.
- [60] C.M. Friend, D.A. Chen, *Polyhedron* 16 (1997) 3165–3175.
- [61] N. Frizi, P. Blanchard, E. Payen, P. Baranek, M. Rebeilleau, C. Dupuy, J.P. Dath, *Catal. Today* 130 (2008) 272–282.
- [62] F.E. Massoth, G. Muralidhar, J. Shabtai, *J. Catal.* 85 (1984) 53–62.
- [63] Z.-D. Huang, W. Bensch, L. Kienle, S. Fuentes, G. Alonso, C. Ornelas, *Catal. Lett.* 122 (2008) 57–67.
- [64] R. Nava, A. Infantes-Molina, P. Castaño, R. Guil-López, B. Pawelec, *Fuel* 90 (2011) 2726–2737.